"FeV–cofactor"–inspired bionic Fe–doped $BiVO_4$ photocatalyst decorated with few layer 2D black phosphorus for efficient nitrogen reduction

Hongda Li,[a,c] Shuai Jian,[a] Boran Tao,[a,c] Guoxiao Xu,[a] Baosheng Liu,[a] Shaonan Gu,[b,*] Guofu Wang,[a,*] Haixin Chang [c,*]

[a] Liuzhou key laboratory for new energy vehicle power lithium battery, School of Electronic Engineering, Guangxi University of Science and Technology, Liuzhou, 545006, China

[b] Key Laboratory of Fine Chemicals in Universities of Shandong, Jinan Engineering Laboratory for Multi–Scale Functional Materials, School of Chemistry and Chemical Engineering, Qilu University of Technology (Shandong Academy of Sciences), Jinan 250353, China

[c] Quantum–Nano Matter and Device Lab, State Key Laboratory of Material Processing and Die & Mould Technology, School of Materials Science and Engineering, Huazhong University of Science and Technology, Wuhan 430074, China

Corresponding authors: hxchang@hust.edu.cn (Haixin Chang); sngu@qlu.edu.cn (Shaonan Gu); gfwang@guet.edu.cn (Guofu Wang)

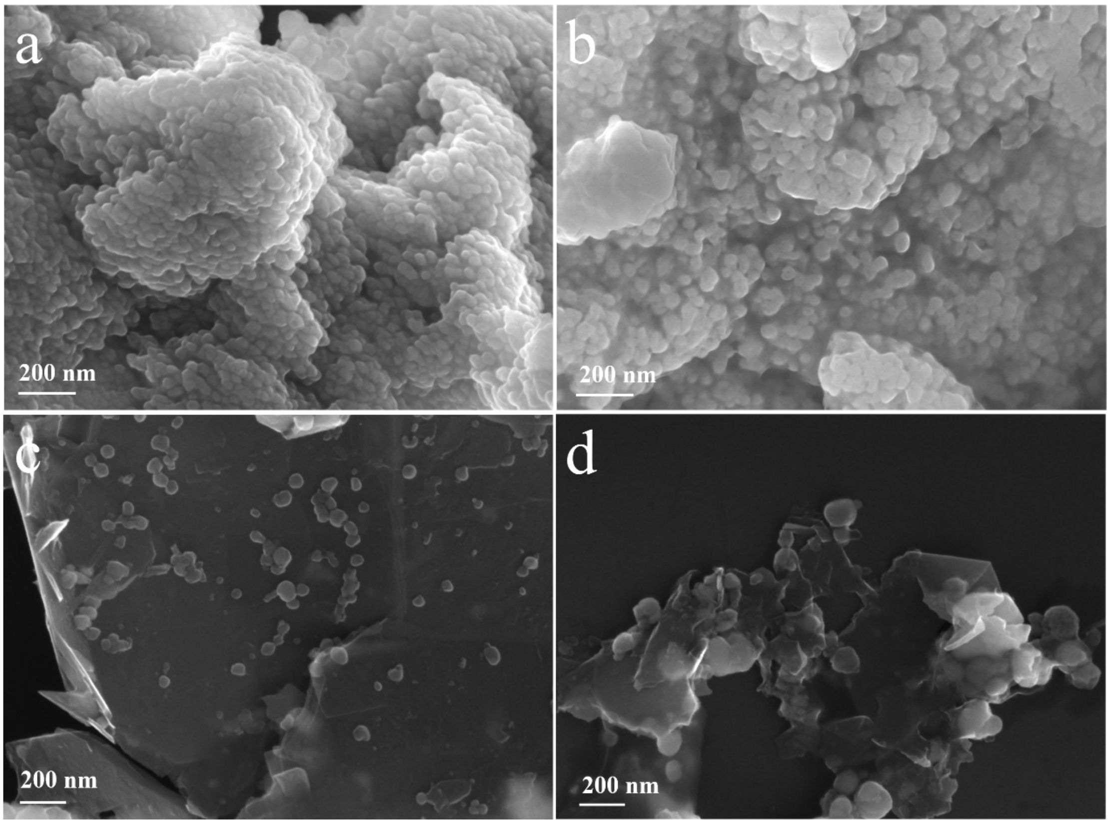

Figure S1. SEM images of (a) $BiVO_4$, (b) $FeBiVO_4$, (c) $FeBiVO_4$-0.05BP and (d) $BiVO_4$-0.05BP.

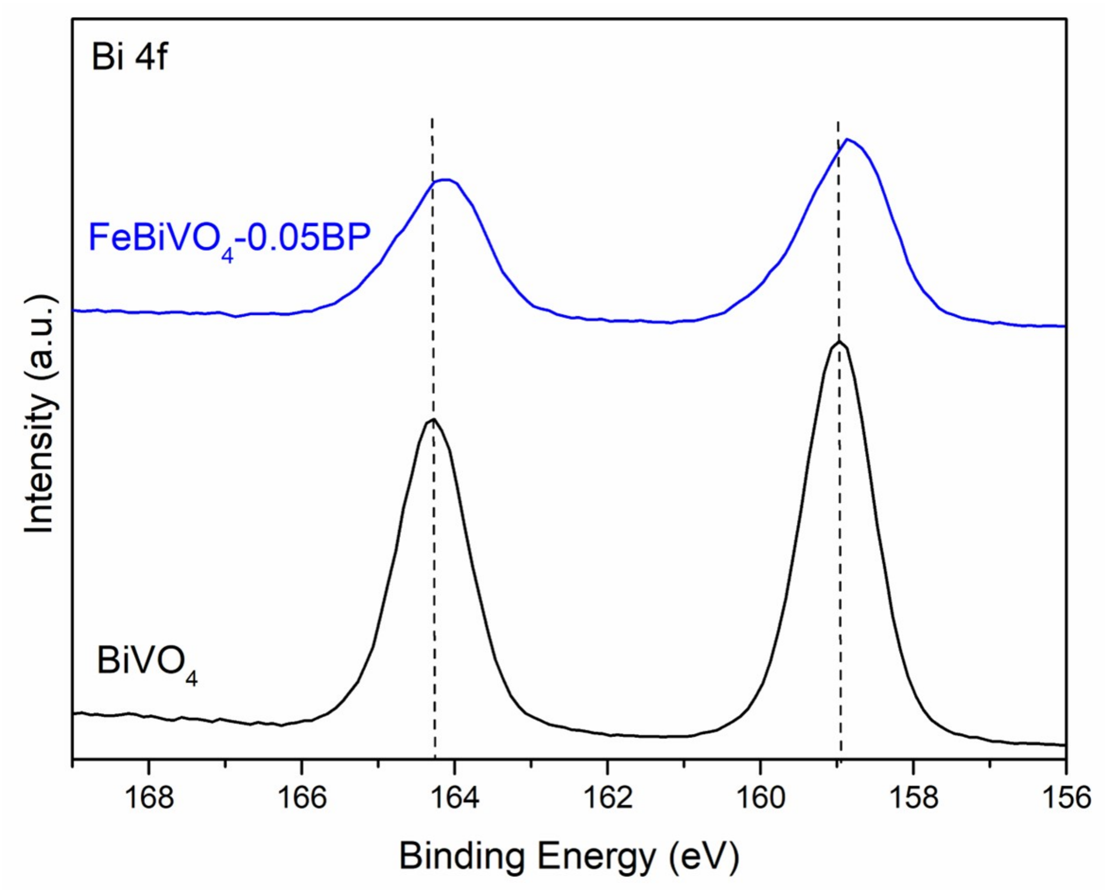

Figure S2. High-resolution XPS of Bi 4*f* for $BiVO_4$ and $FeBiVO_4$-0.05BP.

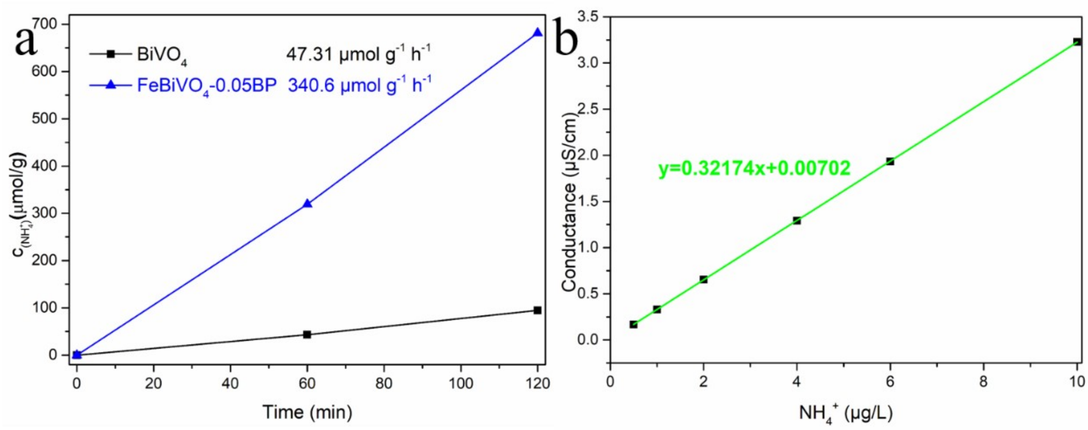

Figure S3. The NH_4^+ amount detected by cation exchange chromatography: (a) photocatalytic N_2 reduction of $BiVO_4$ and $FeBiVO_4$–0.05BP under visible light irradiation; (b) the standard curve.

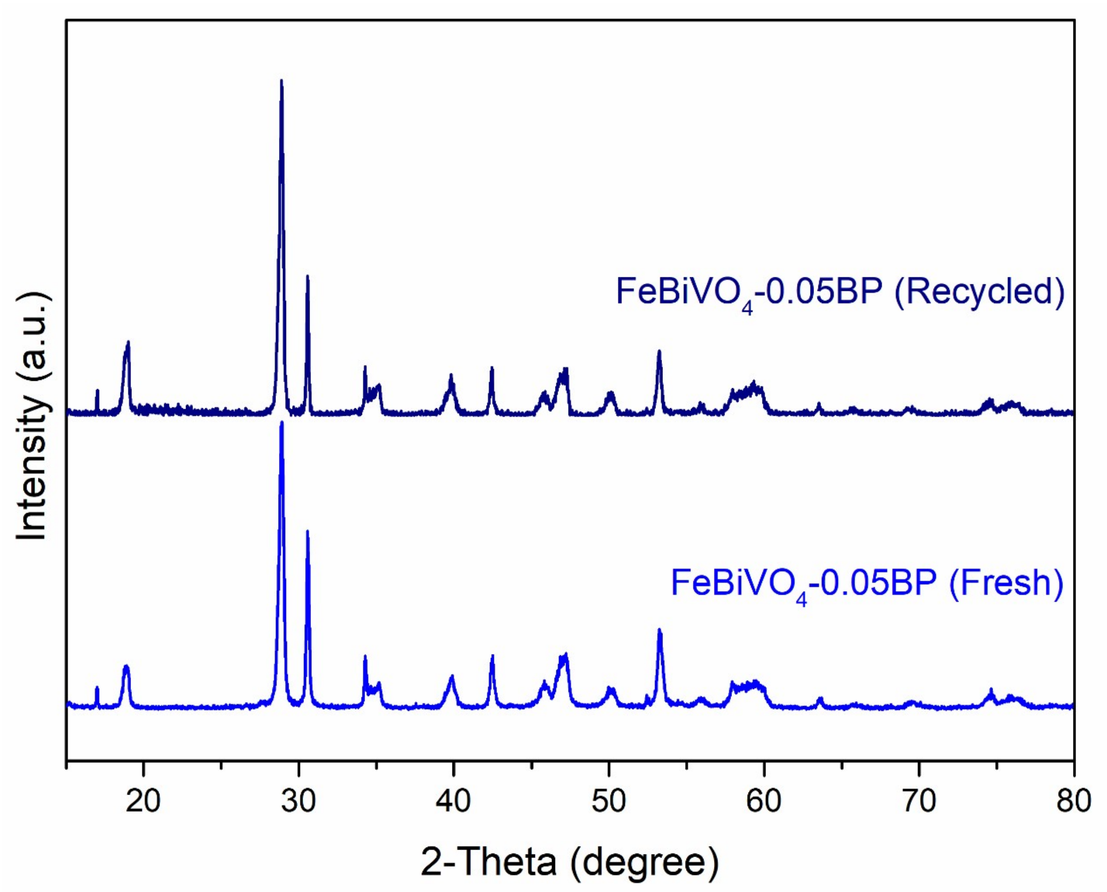

Figure S4. XRD patterns of fresh and recycled $FeBiVO_4$–0.05BP.

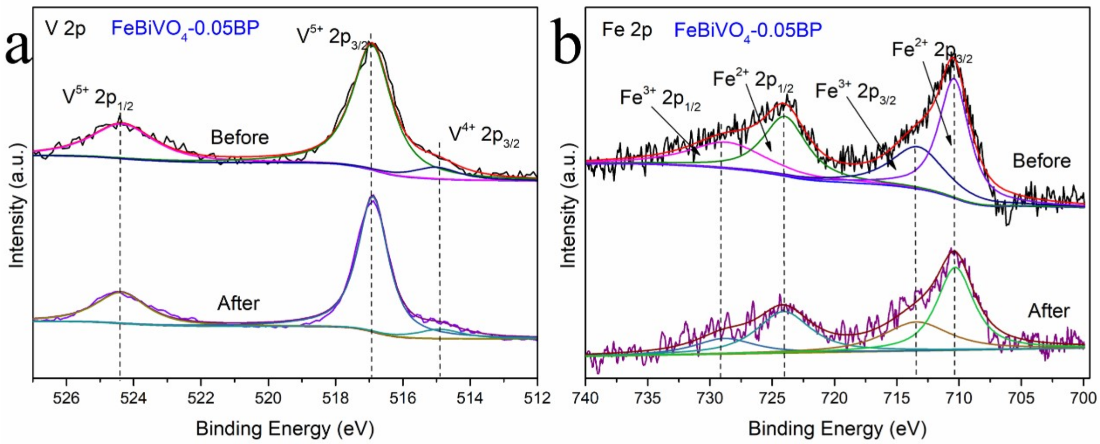

c

Photocatalytic nitrogen reduction reaction	Fe^{3+} (Peak area proportion)	Fe^{2+} (Peak area proportion)	V^{5+} (Peak area proportion)	V^{4+} (Peak area proportion)
Before	40.66%	59.34%	92.96%	7.04%
After	35.08%	64.92%	93.05%	6.95%

Figure S5. Changes of XPS before and after photocatalytic nitrogen reduction reaction: (a) V 2p and (b) Fe 2p; (c) summary of changes in XPS peak areas. There are almost no changes in the valence states of V element, while the number of Fe^{2+} becomes more after photocatalytic nitrogen reduction reaction. This may be due to the presence of electron transfer between redox couples (V^{5+}/V^{4+} and Fe^{3+}/Fe^{2+}) during photocatalytic nitrogen reduction, and the need to reduce part of Fe^{3+} needs to be reduced to Fe^{2+}, thus achieving the redox regulation equilibrium of V^{5+}/V^{4+} and Fe^{3+}/Fe^{2+} and the valence equilibrium between Fe and V ions.

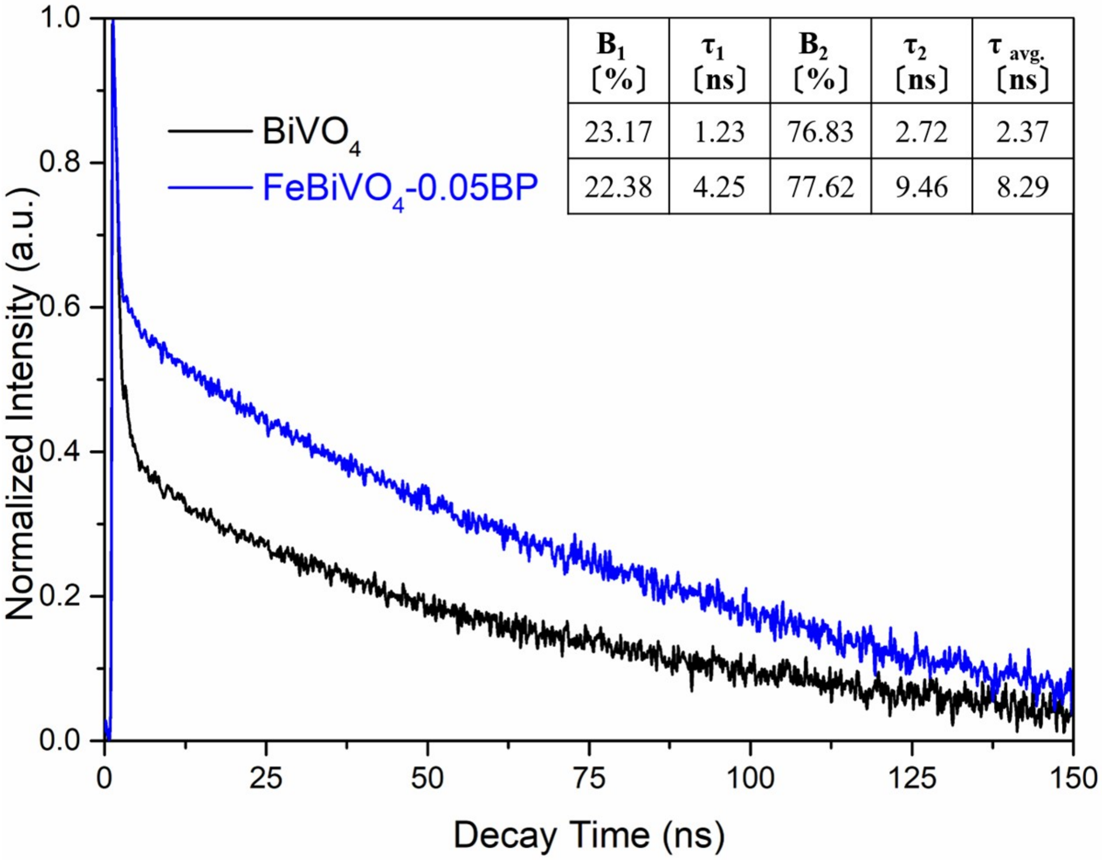

B_1 (%)	τ_1 (ns)	B_2 (%)	τ_2 (ns)	$\tau_{avg.}$ (ns)
23.17	1.23	76.83	2.72	2.37
22.38	4.25	77.62	9.46	8.29

Figure S6. Time–resolved fluorescence decay spectra of $BiVO_4$ and $FeBiVO_4$–0.05BP.

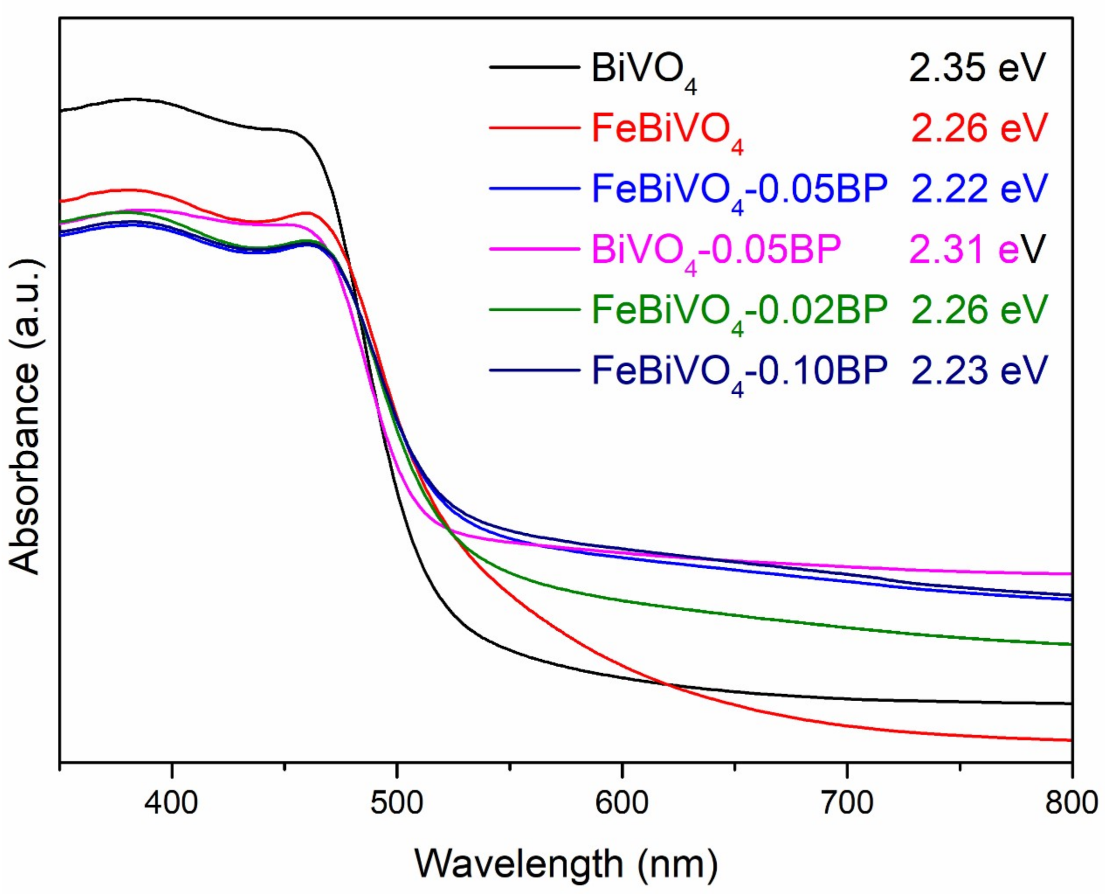

Figure S7. UV–vis diffuse reflectance spectra of $BiVO_4$, $FeBiVO_4$, $BiVO_4$-0.05BP, $FeBiVO_4$-0.05BP, $FeBiVO_4$-0.02BP and $FeBiVO_4$-0.10BP.

Text S1

The corresponding equations (Eq. (3-10)) for the change in Gibbs free energy are as following:

$\triangle G_1 = G(* NN) - G(*) - G(N_2)\#(S1)$

$\triangle G_2 = G(* NNH) - G(* NN) - G(H)\#(S2)$

$\triangle G_3 = G(* NNH_2) - G(* NNH) - G(H)\#(S3)$

$\triangle G_4 = G(* NNH_3) - G(* NNH_2) - G(H)\#(S4)$

$\triangle G_5 = G(* NH) + G(NH_3) - G(* NNH_3) - G(H)\#(S5)$

$\triangle G_6 = G(* NH_2) - G(* NH) - G(H)\#(S6)$

$\triangle G_7 = G(* NH_3) - G(* NH_2) - G(H)\#(S7)$

$\triangle G_8 = G(*) + G(NH_3) - G(* NH_3)\#(S7)$

Table S1. Unit cell parameters of $BiVO_4$ and $FeBiVO_4$.

Samples	**Crystal Vol (Å^3)**	**Lattice Parameters**		
		a (Å)	**b (Å)**	**c (Å)**
$BiVO_4$	310.27	5.197	11.700	5.103
$FeBiVO_4$	308.98	5.182	11.690	5.101

Table S2. Element concentrations (ICP-OES) and BET specific surface areas of $BiVO_4$, $FeBiVO_4$, $FeBiVO_4$-0.05BP and $BiVO_4$-0.05BP.

Samples	**$BiVO_4$**	**$FeBiVO_4$**	**$FeBiVO_4$-0.05BP**	**$BiVO_4$-0.05BP**
Surface areas (m^2 g^{-1})	35.23	34.19	51.84	49.98
Bi (ppm)	284.6	296.9	274.3	286.7
Fe (ppm)	/	1.554	1.442	/
V (ppm)	68.81	74.63	66.79	69.41
P (ppm)	/	/	15.37	16.51
Theoretical Fe/Bi (mol%)	/	2.00	2.00	/
Real Fe/Bi (mol%)	/	1.95	1.96	/
Theoretical P (wt.%)	/	/	5.00	5.00
Real P (wt.%)	/	/	4.29	4.43

Table S3. Photocatalytic nitrogen fixation performance of different catalysts under various reaction conditions.

Catalysts	Scavenger	Light Source	NH_3 generation rate μmol g^{-1} h^{-1}	Reference
$BiVO_4$	None	300 W Xe lamp, λ>400 nm	103.4	S1
Porous C-TiO_2	None	300 W Xe lamp, λ>395 nm	109.3	S2
Fe-$W_{18}O_{49}$-BP	None	500 W Xe lamp	187.6	S3
Ni_2P-BP	Methanol	300 W Xe lamp	6.14	S4
Defect-rich Bi_3O_4Br	None	300 W Xe lamp	50.4	S5
F capped TiO_2	None	300 W Xe lamp	206	S6
Bi_2WO_6-BP	None	300 W Xe lamp	73.6	S7
Gd-Bi_2MoO_6	None	300 W Xe lamp, λ>420 nm	300.15	S8
CdS/WO_3	None	300 W Xe lamp	35.8	S9
$FeBiVO_4$-0.05BP	None	300 W Xe lamp, λ>420 nm	337.9	This work

References

[S1] G. Zhang, Y. Meng, B. Xie, Z. Ni, H. Lu, S. Xia, Precise location and regulation of active sites for highly efficient photocatalytic synthesis of ammonia by facet-dependent $BiVO_4$ single crystals, *Appl. Catal. B: Environ.* 2021, 296, 120379.

[S2] Q. Han, C. Wu, H. Jiao, R. Xu, Y. Wang, J. Xie, Q. Guo, J. Tang, Rational Design of High-Concentration Ti^{3+} in Porous Carbon-Doped TiO_2 Nanosheets for Efficient Photocatalytic Ammonia Synthesis, *Adv. Mater.* 2021, 33, 2008180.

[S3] G. Dong, X. Huang, Y. Bi, Anchoring Black Phosphorus Quantum Dots on Fe-Doped $W_{18}O_{49}$ Nanowires for Efficient Photocatalytic Nitrogen Fixation, *Angew. Chem. Int. Edit.* 2022, 61, e202204271.

[S4] Z.-K. Shen, M. Cheng, Y.-J. Yuan, L. Pei, J. Zhong, J. Guan, X. Li, Z.-J. Li, L. Bao, X. Zhang, Z.-T. Yu, Z. Zou, Identifying the role of interface chemical bonds in activating charge transfer for enhanced photocatalytic nitrogen fixation of Ni_2P-black phosphorus photocatalysts, *Appl. Catal. B: Environ.* 2021, 295, 120274.

[S5] J. Di, J.X. Xia, M. F. Chisholm, J. Zhong, C. Chen, X. Z. Cao, F. Dong, Z. Chi, H.L. Chen, Y. X. Weng, J. Xiong, S. Z. Yang, H. M. Li, Z. Liu, S. Dai, Defect-tailoring mediated electron-hole separation in single unit cell Bi_3O_4Br nanosheets for boosting photocatalytic hydrogen evolution and nitrogen fixation, *Adv. Mater.* 2019, 31, 1807576.

[S6] R. Guan, D. Wang, Y. Zhang, C. Liu, W. Xu, J. Wang, Z. Zhao, M. Feng, Q. Shang, Z. Sun, Enhanced photocatalytic N_2 fixation via defective and fluoride modified TiO_2 surface. *Appl. Catal. B: Environ.* 2021, 282, 119580.

[S7] L. Liu, J. Liu, K. Sun, J. Wan, F. Fu, J. Fan, Novel phosphorus-doped Bi2WO6 monolayer with oxygen vacancies for superior photocatalytic water detoxication and nitrogen fixation performance, *Chem. Eng. J.* 2021, 411, 128629.

[S8] H. Li, H. Zhao, C. Li, B. Li, B. Tao, S. Gu, G. Wang, H. Chang, Redox regulation of photocatalytic nitrogen reduction reaction by gadolinium doping in two-dimensional bismuth molybdate nanosheets, *Appl. Surf. Sci.* 2022, 600, 154105.

[S9] P. Xia, X. Pan, S. Jiang, J. Yu, B. He, P. M. Ismail, W. Bai, J. Yang, L. Yang, H. Zhang, M. Cheng, H. Li, Q. Zhang, C. Xiao, Y. Xie, Designing a Redox Heterojunction for Photocatalytic

"Overall Nitrogen Fixation" under Mild Conditions, *Adv. Mater.* 2022, 34, 2200563.